International Conference on Space Optics—ICSO 2022

Dubrovnik, Croatia

3–7 October 2022

Edited by Kyriaki Minoglou, Nikos Karafolas, and Bruno Cugny,

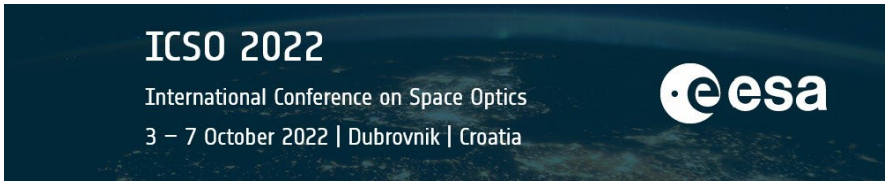

Scene-based wavefront correction using SPGD algorithm for high resolution Earth observation

International Conference on Space Optics — ICSO 2022, edited by Kyriaki Minoglou, Nikos Karafolas, Bruno Cugny, Proc. of SPIE Vol. 12777, 127774A · © 2023 ESA and CNES · 0277-786X · doi: 10.1117/12.2690817

Scene-based wavefront correction using SPGD algorithm for high-resolution Earth observation

M. Hirose*[a], N. Miyamura[b], S. Sato[a], T. Mizutani[a], T. Kimura[a]
[a]Japan Aerospace Exploration Agency, 2-1-1, Sengen, Tsukuba, Ibaraki, 305-8505 Japan;
[b]Department of Interdisciplinary Science and Engineering, Meisei University,
2-1-1, Hodokubo, Hino, Tokyo, 191-8506 Japan

ABSTRACT

Model-free image-based wavefront correction is a useful technique in resource-limited spaceborne imaging systems used for Earth observation. However, such an approach is difficult because correction performance depends on selection of the measured scenes and the evaluation metric. In this study, the relationship is experimentally and numerically investigated using the stochastic parallel gradient descent (SPGD) algorithm. As a result, the combination of deviation-based metrics and scenes with distinct structures was found to facilitate wavefront correction. The results also show that the present approach is useful in not only monolithic but also segmented mirror optics. The proposed method will contribute to realize on-orbit wavefront-sensorless aberration removal required in near-future high-resolution Earth observation systems.

Keywords: Segmented mirror optics, adaptive optics, wavefront correction, multivariable optimization

1. INTRODUCTION

A demand for responsive large-scale land observation from orbiting satellites is emerging for such purposes as mitigating human suffering in catastrophic disasters. A geostationary satellite with a large-sized optical imager is one of the promising solutions to meet this need. We have studied the feasibility of a geostationary satellite with a 3.6-meter-diameter optical telescope [1,2]. The telescope utilizes a segmented mirror strategy, and thus the primary mirror is divided into six hexagonal mirror segments to suppress the total weight of the optics. Given the increasing size of the mirror aperture, the on-orbit wavefront control technique plays an important role, particularly in segmented mirror optics, to achieve diffraction-limited imaging performance. In resource-limited spaceborne imaging systems, use of the wavefront-sensorless aberration correction technique is desirable. The phase diversity (PD) method enables parametric aberration retrieval from the measured ground scenes [3]. This approach involves at least two measurements of the identical field-of-view by introducing the known wavefront diversities, and is known to be useful in both monolithic and segmented aperture systems. However, it requires accurate modeling of the measurement systems and conditions to obtain sufficient precision in aberration retrieval. Therefore, the model-based approaches would suffer from on-orbit modeling errors.

Model-free correction techniques based on multivariable optimization algorithms allow us to avoid any modeling difficulties. In these approaches, wavefront error is corrected by iteratively optimizing a cost function defined from the measured images. The cost function is an evaluation metric of wavefront aberration remaining in the imaging systems. There are some optimization algorithms for correcting wavefront error [4,5]. Among them, the stochastic parallel gradient descent (SPGD) algorithm has been extensively studied due to its stable convergence property [6]. However, previous studies using the SPGD algorithm have mainly observed a point light source or samples with binarized structures such as test charts. Therefore, the correction performance using an extended scene as an observation target has not been fully investigated. Moreover, the relationship between convergence speed, the cost function, and scenes remains unclear. To apply the SPGD algorithm to spaceborne imaging systems for Earth observation, it is crucial to understand the optimization behaviors when observing extended aerial scenes. In this study, we first formulate the SPGD algorithm and propose potential candidates for the cost functions to achieve efficient aberration removal. Next, we build an optical testbed that can simulate aberrated imaging systems equipped with a deformable mirror. Then, demonstration experiments are conducted with the proposed cost functions and aerial scenes. Finally, numerical simulations are performed to evaluate the feasibility of the SPGD algorithm in segmented mirror optics for Earth observation [7].

*hirose.makoto@jaxa.jp; phone 81 70-1170-3354

2. PRINCIPLE

Earth observation by spaceborne optical imagers is described by incoherent imaging systems. Thus, the image formation process is written as:

$$I(\mathbf{r}) = \int_{\lambda_1}^{\lambda_2} s(\lambda) I_0(\mathbf{r}, \lambda) \otimes |h(\mathbf{r}, \lambda)|^2 d\lambda + n(\mathbf{r})$$

where $\mathbf{r}$ is real-space coordinates, s is spectral intensity, I_0 is the ground truth, h is the optical response, λ_1 and λ_2 are minimum and maximum wavelengths in the spectral range, respectively, and n is observation noise. The optical response h at a specific wavelength is related to the wavefront aberration W as:

$$h(\mathbf{r}) = \mathrm{F}[|P(\mathbf{k})| \exp\{iW(\mathbf{k})\}]$$

where $\mathbf{k}$ is pupil-space coordinates, and F denotes the Fourier transform operator. In most axisymmetric optical systems, Zernike polynomials are a useful basis to express the wavefront aberration as [8]:

$$W(\mathbf{k}) = \sum_{m=0}^{M} a_m Z_m(\mathbf{k})$$

where a_m is the aberration coefficient, M is maximum aberration mode, and Z_m is each aberration term. The image-based wavefront correction aims to control actuators of corrective devices based on the measured intensity data to reduce the aberration.

The SPGD algorithm is one of the most promising approaches for stable image-based wavefront correction. The variable is the control vector $\mathbf{u}$ of the corrective device used for wavefront control. The control vector is repeatedly modified until a cost function defined from the measured images converges. The cost function is an indicator used to evaluate the remaining aberration in the optical systems. In the SPGD algorithm, the parameters are revised based on variation of the cost function evaluated by introducing positive and negative wavefront perturbation. The perturbation is added by intentionally actuating the corrective device. The mathematical expression at the nth iteration in the SPGD algorithm is written as:

$$\mathbf{u}_{n+1} = \mathbf{u}_n - \gamma\{J(\mathbf{u}_n + \Delta\mathbf{u}) - J(\mathbf{u}_n - \Delta\mathbf{u})\}\Delta\mathbf{u}$$

where γ is the feedback parameter, J is the cost function, and $\Delta\mathbf{u}$ is the perturbation vector. To accelerate wavefront correction, it is effective to provide the perturbation in the form of Zernike polynomials as:

$$\Delta\mathbf{u} = \sum_{m=0}^{M} \Delta a_m Z_m(\mathbf{k})$$

where $\Delta\mathbf{a}$ is stochastically determined aberration coefficients. If the corrective device has a large number of actuators, this treatment greatly improves the correction speed. The convergence of the SPGD algorithm depends on selection of the cost function. Given the implementation of the SPGD algorithm on space optics, the calculation form must be simple. Here, we introduce the following metrics as:

$$J_1 = m[I^2(\mathbf{r})]$$

$$J_2 = \sigma[I(\mathbf{r})]$$

$$J_3 = \sigma[I^2(\mathbf{r})]$$

$$J_4 = m\left[\sqrt{\left(\frac{\partial I(\mathbf{r})}{\partial x}\right)^2 + \left(\frac{\partial I(\mathbf{r})}{\partial y}\right)^2}\right]$$

where σ and m denote the standard deviation and average of the given data, respectively. The intensity-based J_1 metric has been most widely used for wavefront correction, whereas deviation-based J_2 or J_3 metrics have not been often used. The J_4 metric evaluates the spatial gradient of the measured image. The difference from selection of the cost function has yet to be compared, at least not in experiments. In the subsequent wavefront correction, the convergence performance for each cost function was compared.

3. SCENE-BASED WAVEFRONT CORRECTION

3.1 Experimental setup

Figure 1 (a) shows the experimental setup for wavefront correction using the SPGD algorithm. A halogen lamp was used as an incoherent light source, and image films were placed for the observation scenes. The pictures on the image films were the city and harbor scenes captured by our aircraft observations in Japan. The light that passed films was collimated by an objective lens, then incident on the membrane deformable mirror for wavefront control. The rear surface of the membrane mirror is supported by two-dimensionally aligned 140 MEMS actuators. The actuator pitch is 400 μm, and the aperture is 4.4 mm. The reflected wavefront finally formed the film images on the image sensor. The exposure time was set to be 50 ms throughout the experiments.

Figure 1 (b) shows the measured city and harbor images without any intentional wavefront aberration, and their signal-to-noise ratio was sufficient for the experiments. The J_1–J_4 metrics for these images were used when calculating normalized cost functions J_w/J_{wo}, where J_w is the metric of an aberrated image and J_{wo} is the metric of an aberration-free image. The city scene involves many distinct building structures, while the harbor scene is more textureless. In wavefront correction with the SPGD algorithm, once the aberration was introduced on the deformable mirror, the perturbation was added for the optimizations. Figure 1 (c) shows the initial aberration voltage maps applied to the MEMS deformable mirror. Both aberration maps were composed of Z_3–Z_{14} mixture modes. Condition 1 was used for the city film measurements; Condition 2 was used for the harbor film measurement. Based on the deflection curve of the MEMS actuators, the initial wavefront error over the effective aperture was calculated to be 155 nm rms for Condition 1 and 269 nm rms for otherwise.

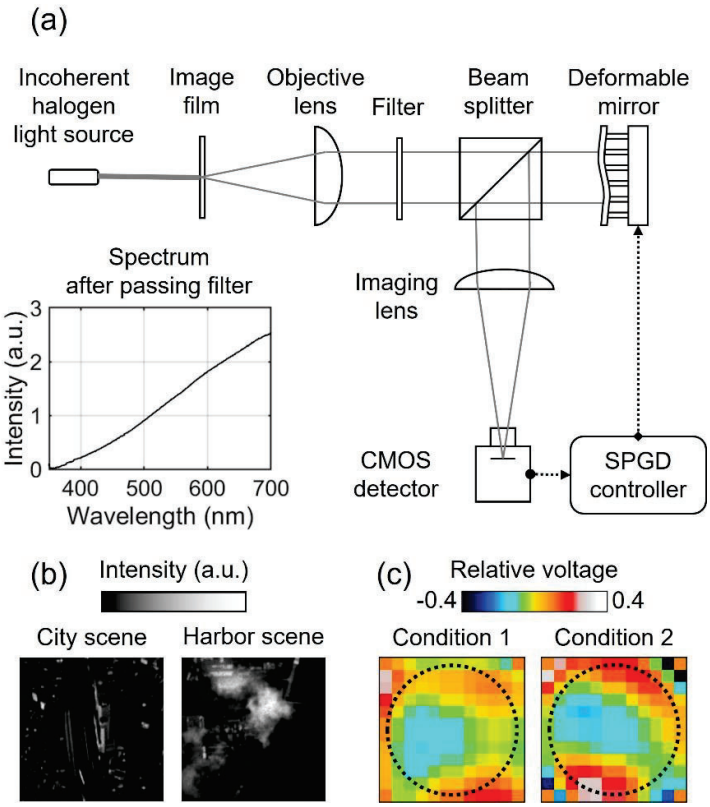

Fig. 1. (a) Experimental layout for wavefront correction using the SPGD algorithm. The inset graph displays the spectrum that contributed to image formation. Wavelength above 700 nm was cut out using the infrared filter. (b) The city and harbor images without intentional aberration. (c) Input aberration patterns to the MEMS deformable mirror. The dashed circle represents the effective aperture of the mirror.

3.2 Experimental results

Figure 2 (a) shows the city image before and after performing the SPGD algorithm with the deviation-based J_3 metric. For the aberrated image, the imaging quality was severely degraded, and the detailed structures were no longer resolved. Meanwhile, the corrected image after 300 iterations was comparable to the original image. The final flatness of the MEMS deformable mirror was 41.0 nm rms, which is smaller than the initial flatness value. The residual flatness potentially includes the wavefront error caused by the initial misalignment of optics such as defocus. Indeed, the final normalized J_3 metric exceeded unity slightly, meaning that the image quality of the final image would be better than the image captured with a flat mirror surface. Figure 2 (b) compares the convergence plots when using four cost functions. With any cost function, all metrics finally reached almost unity, which means wavefront correction succeeded in every case. However, the convergence speed was different. The deviation-based J_3 metric and the gradient-based J_4 metric exhibited faster convergence, while the intensity-based J_1 metric, which was mostly used in previous studies, resulted in a slower trend. These convergence plots revealed that the cost function with larger initial drops from unity is more capable of detecting and correcting the wavefront aberration.

Figure 3 (a) represents wavefront correction using the harbor scene as an observation target. Although the initial aberrated image was significantly blurred, the SPGD algorithm successfully recovered the image quality. The final flatness of the MEMS deformable mirror was 46.3 nm rms (similar to the flatness level in the previous experiment). As shown in Fig. 3 (b), however, the convergence rate became slower for every cost function. This indicated that the use of textureless scenes makes wavefront correction more challenging as the image quality of textureless images is less sensitive to the existence of the wavefront aberration. A similar scene dependence is also reported in wavefront sensing by the scene-based Shack–Hartmann sensor [9]. It is noted that the behavior of the metric evolution was also different between the deviation-based J_3 metric and the gradient-based J_4 metric. Optimization with the J_4 metric suffered from updating the deformable mirror at the beginning of the iteration. The gradient-based metric is only sensitive to the adjacent pixel values. Thus, for the textureless scene contaminated by observation noise, wavefront correction with the J_4 metric became difficult. Conversely, the deviation-based metric showed a trend similar to that of the city film experiment. Therefore, the deviation-based metric is found to be useful for versatile scenes.

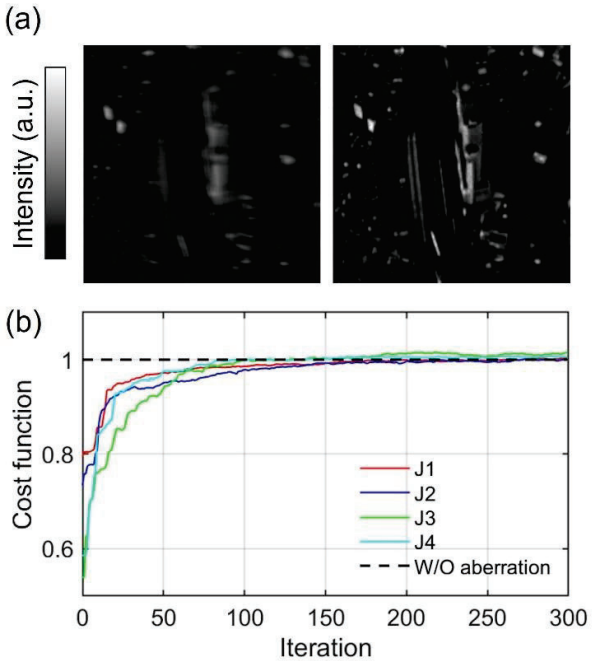

Fig. 2. Experimental wavefront correction with the city scene. (a) Measured film image before (left) and after (right) performing the SPGD algorithm with the deviation-based J_3 metric. The initial and final flatness of the MEMS deformable mirror was 155 nm rms and 41.0 nm, respectively. (b) Convergence curves of each normalized cost function.

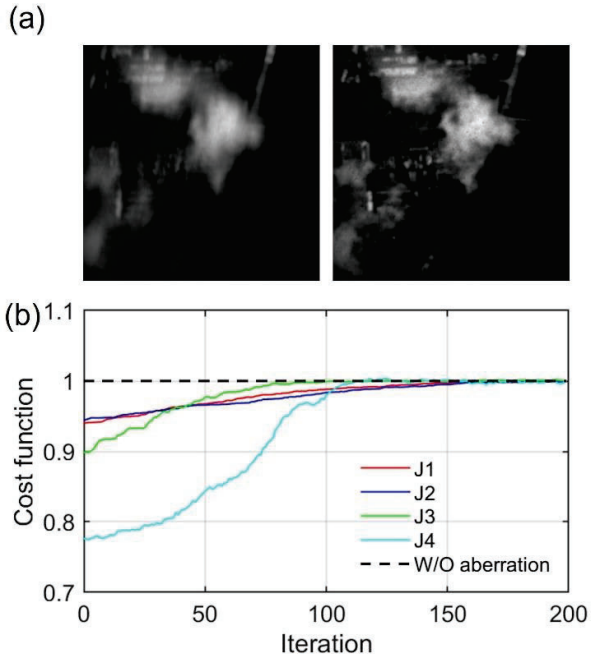

Fig. 3. Experimental wavefront correction with the harbor scene. (a) Measured film image before (left) and after (right) performing the SPGD algorithm with the deviation-based J_3 metric. The initial and final flatness of the MEMS deformable mirror was 269 nm rms and 46.3 nm, respectively. (b) Convergence curves of each normalized cost function.

3.3 Numerical simulation for segmented mirror optics

Numerical simulations were performed to evaluate the feasibility of the SPGD algorithm in the segmented mirror optics. In segmented mirror systems, wavefront correction needs several phasing steps as seen in the James Webb Space Telescope [10]. This simulation dealt with the fine phasing that entails final adjustments of primary mirror segments. The simulated primary mirror consisted of six hexagonal segments, and the aberration loaded at each segment was a random mixture of Z_0–Z_{14} aberration terms. Thus, the piston-tip-tilt misalignment was included in the simulation. Namely, the wavefront aberration of the primary mirror with six segments was expressed as:

$$W(\mathbf{k}) = \sum_{n=1}^{6} \sum_{m=0}^{14} a_{m,n} Z_m(\mathbf{k} - \mathbf{r}_n)$$

where $\mathbf{r}_n$ is the distance from the pupil center for the nth mirror segment. In this simulation, it was assumed that the corrective device had the capability of controlling the same aberration modes, and the perturbation used in the optimization was also defined by Z_0–Z_{14} modes. Another aerial scene was selected as the observation target, and Gaussian noise was added to every measurement to make the signal-to-noise ratio less than 100.

Figure 4 (a) shows the initial aberration and the measured scene. The initial wavefront error over the effective aperture was 0.245 λ rms, and the corresponding measured scene was distorted. Starting from this condition, the SPGD algorithm with the deviation-based metric was applied until the cost function converged. For aberration removal, 87 parameters were optimized. Figure 4 (b) presents the post-correction results. The wavefront error decreased to 8.17×10^{-3} λ rms, and the image showed detailed features again. Moreover, the final normalized cost function was recovered to 1.00. Figure 4 (c) shows the convergence curves. The optimization was performed five times independently to see the stochastic variation. In all trials, the optimizations converged with almost 2,000 iterations. Although the iteration number until convergence largely increased, wavefront correction using the SPGD algorithm was effective in segmented mirror optics.

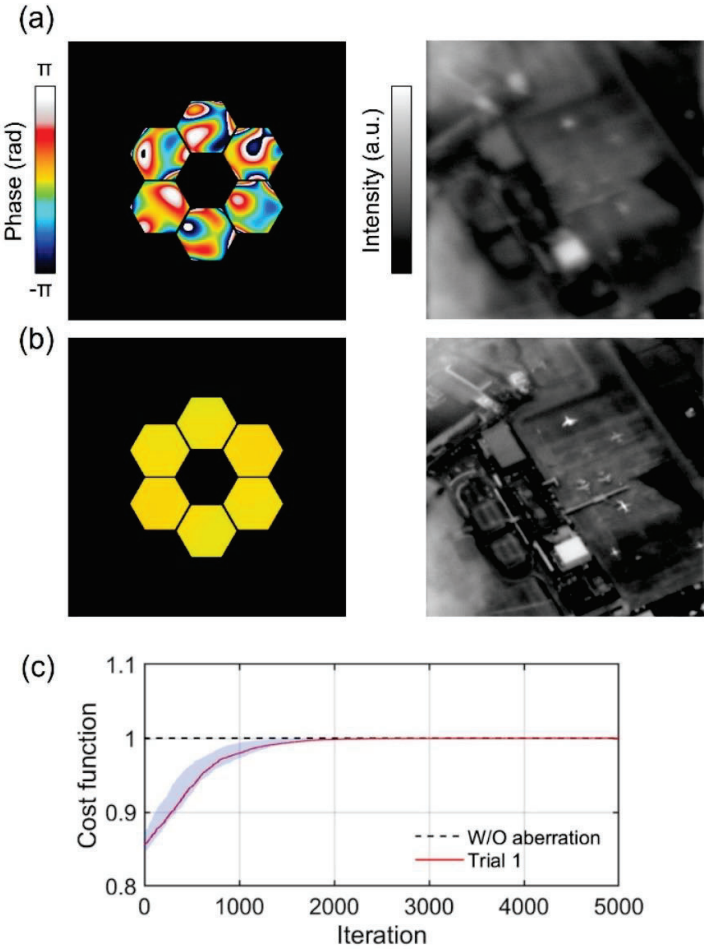

Fig. 4. Numerical wavefront correction in segmented mirror optics. (a) Pupil phase (left) and measured scene (right) before correction with the deviation-based metric. (b) The same dataset after correction. (c) Convergence curves. Blue-colored area represents the range of cost function during five independent optimizations.

4. SUMMARY

In this paper, we experimentally compared several cost functions used in the SPGD algorithm for high-resolution optical remote sensing. We first built a testbed imaging system equipped with a MEMS deformable mirror for wavefront control. In the testbed experiments, the deviation-based and gradient-based metrics showed a better capability of correcting wavefront aberration than the most widely used intensity-based cost function. Moreover, the gradient-based cost function was found to suffer from correctly updating the mirror shape when textureless scenes are measured. Consequently, the deviation-based cost function was found to be effective for versatile scenes. Scenes with distinct structures also facilitated wavefront correction. We then performed numerical simulations for wavefront correction in segmented mirror optics. The simulated optics consisted of circularly aligned six hexagonal mirrors and a central obscuration. Although a higher iteration count was inevitable, the SPGD algorithm finally found the optimal phase map to cancel out the initially applied aberration. For efficient wavefront correction, it would be useful to perform the model-based approach such as phase diversity in advance.

The proposed approach is especially useful in our geostationary optical telescope satellite since the observation areas can be fixed [1]. The remaining challenge is the feasibility of wavefront correction using scenes with moving objects, such as vehicles and clouds. The conventional SPGD algorithm requires observation of stationary scenes during the measurements. Besides, decreasing the computational cost is also important for on-board data processing. After overcoming these technical issues, the proposed approach allows us to realize high-resolution remote sensing systems with large monolithic or segmented mirror optics.

REFERENCES

[1] T. Mizutani et al., Conceptual study of 3.5-m segmented mirror for geostationary earth observation satellite. Proc. SPIE **10781**, 10 pages, (2018).
[2] T. Mizutani et al., Geostationary earth observation system concept by 3.6-meter synthetic aperture imaging. Proc. SPIE **11858**, 8 pages (2021).
[3] R. A. Gonsalves, Phase retrieval and diversity in adaptive optics. Opt. Eng. **21**, 829−832 (1982).
[4] O. Kazasidis et al., Extended-image-based correction of aberrations using a deformable mirror with hysteresis. Opt. Express **26**, 27161−27178 (2018).
[5] T. Yeminy and O. Katz, Guidestar-free image-guided wavefront shaping. Sci. Adv. **7**, eabf5364 (2021).
[6] M. A. Voronstov and V. P. Sivoken, Stochastic parallel-gradient-decent technique for high-resolution wavefront distortion correction. J. Opt. Soc. Am. A **15**, 2745−2758 (1998).
[7] M. Hirose et al., Deviation-based wavefront correction using the SPGD algorithm for high-resolution optical remote sensing. Appl. Opt. **61**, 6722−6728 (2022).
[8] L. N. Thibos et al., Standards for Reporting the Optical Aberrations of Eyes. in Vision Science and its Applications, (Optica Publishing Group, 2000), p. SuC1.
[9] M. Rais et al., Improving wavefront sensing with a Shack–Hartmann device. Appl. Opt. **55**, 7836–7846 (2016).
[10] D. S. Acton et al., Wavefront sensing and controls for the James Webb Space Telescope. Proc. SPIE **8442**, 877–887 (2012).